International Journal of Nanomedicine

Dovepress
open access to scientific and medical research

Open Access Full Text Article

ORIGINAL RESEARCH

The Remarkable Anti-Breast Cancer Efficacy and Anti-Metastasis by Multifunctional Nanoparticles Co-Loading Squamocin, R848 and IR 780

Xi Wang[1], Xinxin Liu[1], Yaoyao Guo[1,2], Tingting Gong[1], Wenmin Lu[1,3], Meihua Han[1], Yifei Guo[1], Xiangtao Wang[1]

[1]Institute of Medicinal Plant Development, Chinese Academy of Medical Sciences and Peking Union Medical College, Beijing, People's Republic of China; [2]College of Traditional Chinese Medicine, Shenyang Pharmaceutical University, Shenyang, Liaoning Province, People's Republic of China; [3]College of Pharmacy, Heilongjiang University of Chinese Medicine, Harbin, Heilongjiang Province, People's Republic of China

Correspondence: Xiangtao Wang, Institute of Medicinal Plant Development, Chinese Academy of Medical Sciences and Peking Union Medical College, No. 151, Malianwa North Road, Haidian District, Beijing, 100193, People's Republic of China, Tel +86-10-57833266, Email xtaowang@163.com

Background: Breast cancer is a heterogeneous disease globally accounting for approximately 1 million new cases annually. Chemotherapy remains the main therapeutic option, but the antitumor efficacy needs to be improved.

Methods: Two multifunctional nanoparticles were developed in this paper using oleic acid and $mPEG_{2k}$-PCL_{2k} as the drug carriers. Squamocin (Squ) was employed as a chemotherapeutic agent. Resiquimod (R848) or ginsenoside Rh2 was co-encapsulated in the nanoparticles to remold the immunosuppressive tumor microenvironment, and IR780 was coloaded as a photosensitizer to realize photothermal therapy.

Results: The obtained Squ-R848-IR780 nanoparticles and Squ-Rh2-IR780 nanoparticles were uniformly spherical and approximately (162.200 ± 2.800) nm and (157.300 ± 1.1590) nm, respectively, in average diameter, with good encapsulation efficiency (above 85% for each drug), excellent stability in various physiological media and high photothermal conversion efficiency (24.10% and 22.58%, respectively). After intravenous administration, both nanoparticles quickly accumulated in the tumor and effectively enhanced the local temperature of the tumor to over 45 °C when irradiated by an 808 nm laser. At a low dose of 0.1 mg/kg, Squ nanoparticles treatment alone displayed a tumor inhibition rate of 55.28%, pulmonary metastasis inhibition rate of 59.47% and a mean survival time of 38 days, which were all higher than those of PTX injection (8 mg/kg) (43.64%, 25 days and 37.25%), indicating that Squ was a potent and effective antitumor agent. Both multifunctional nanoparticles, Squ-Rh2-IR780 nanoparticles and Squ-R848-IR780 nanoparticles, demonstrated even better therapeutic efficacy, with tumor inhibition rates of 90.02% and 97.28%, pulmonary metastasis inhibition rates of 95.42% and 98.09, and mean survival times of 46 days and 52 days, respectively.

Conclusion: The multifunctional nanoparticles coloaded with squamocin, R848 and IR 780 achieved extraordinary therapeutic efficacy and excellent antimetastasis activity and are thus promising in the future treatment of breast tumors and probably other tumors.

Keywords: breast cancer, multifunctional nanoparticle, antitumor efficacy, antimetastasis, combined therapy

Introduction

Cancer is a complex disease that involves a combination of abnormal physiological processes and affects multiple life activities,[1] including DNA repair, apoptosis and immune function regulation.[2–4] Currently, chemotherapy remains the main therapeutic option, including taxane- and anthracycline-based treatments for breast cancer.[5] There is not only the lack of poor targeting but also the occurrence of drug resistance.[6] With the support of abnormal signal transduction pathways, tumor cells hijack and manipulate a variety of biological activities at the same time to achieve proliferation, metastasis and immune escape,[7] making cancer one of the most challenging diseases. Nanoparticles (NPs) provide a variety of advantages for cancer treatment and have been shown to be effective in the delivery of hydrophobic agents,

Received: 8 December 2023
Accepted: 10 May 2024
Published: 23 May 2024

protecting biologically sensitive goods and promoting the controlled release of drugs.[8–11] NPs are also a reliable platform to achieve tumor monitoring and microenvironment remodeling.[12] In addition, the nanoparticle carrier itself can also stimulate the immune response.[13] Near infrared (NIR) light-induced optical diagnosis and treatment is noninvasive and has good safety and adaptability; thus, it has been widely studied recently.[14] Photothermal therapy (PTT), photodynamic therapy (PDT) and light-triggered drug release have also become research hotspots. IR780, a hydrophobic NIR fluorescent dye for in vivo imaging, is also often encapsulated into nanoparticles as a photosensitizer for PTT and PDT.[15,16] However, the immune stimulation induced by PTT alone is usually not strong and insufficient for tumor treatment.[17]

Immunoregulators are substances that play an auxiliary role in nonspecific changes or enhance the specific immune response to antigens.[18] Resiquimod (R848, Figure 1) is an agonist of Toll-like receptor (TLR) 7/8, triggering extensive activation of innate immune cells and regulating immune suppression.[19] Gisenoside Rh2 (Figure 1) is a naturally resourced saponin that displays a strong immunoregulatory effect.[20,21] Such immunoregulators are able to amplify the body's specific response to these tumor antigens through polarizing tumor-associated macrophages (TAMs) from the M2 phenotype to the M1 phenotype, inducing the secretion of proinflammatory cytokines and chemokines, promoting the maturation of dendritic cells and improving their antigen presentation ability. Such a specific antitumor response can not only inhibit the recurrence of the primary tumor but also slow down or even eradicate the growth of metastatic tumors.[22] The combined use of immunoregulators with chemotherapeutic agents was reported to be able to induce more powerful tumor immunogenicity.[23]

Squamocin (Figure 1) is a lactone compound with potent and broad-spectrum antitumor activity isolated from *Annona squamosa* seeds. It inhibits cell cycle arrest and apoptosis by specifically inhibiting NADH-ubiquinone oxidoreductase and cytoplasmic membrane NADH oxidase in the mitochondria of cancer cells and decreasing ATP production, resulting in tumor cell death[24,25] and the avoidance of multidrug resistance. Squ has a potent killing effect on a variety of tumor cells,[26] with an IC_{50} value at the nM level,[27] which is 10–100 times higher than many first-line antitumor drugs, such as doxorubicin and paclitaxel.[28] Usually, a very low dose of Squ can produce a significant antitumor effect in vivo.

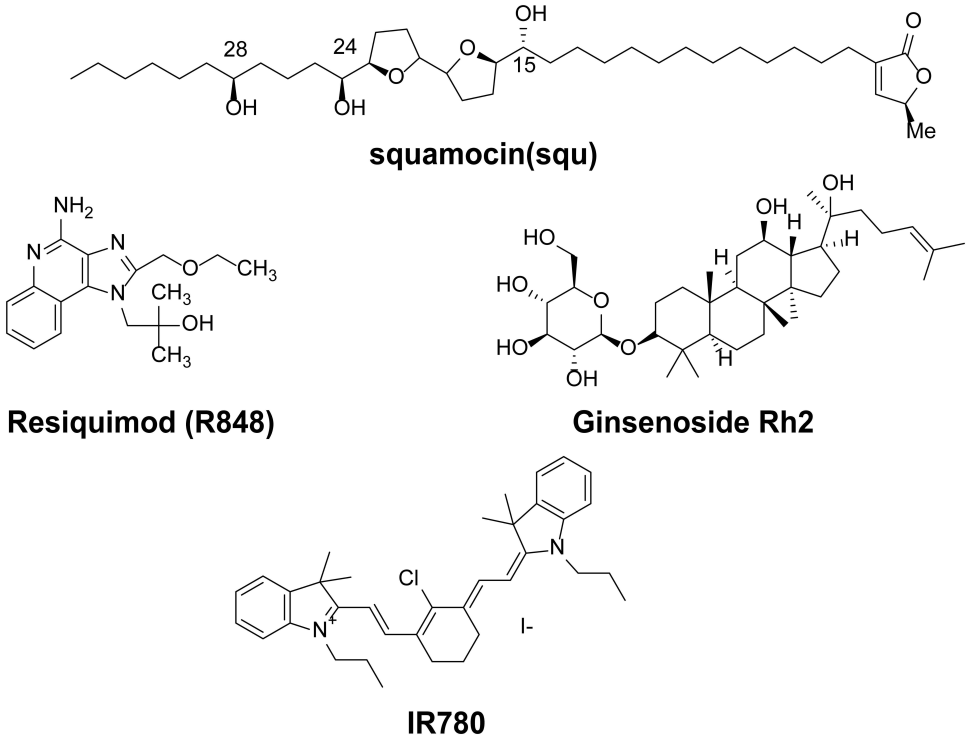

Figure 1 The chemical structure of squanmocin, R848, ginsenoside Rh2 and IR780.

In this paper, two multifunctional NPs integrating chemotherapy, photothermal therapy, immunoregulation and biological imaging, namely, Squ-R848-IR780 NPs and Squ-Rh2-IR780 NPs, were prepared using oleic acid and $mPEG_{2k}$-PCL_{2k} as drug carriers. Both NPs demonstrated high accumulation in tumors and a significant synergistic effect, with the tumor inhibition rate (TIR) as high as 97.28% and a PMIR as high as 98.09%.

Materials and Methods

Materials

Squamocin was isolated and purified from the seeds of *Annona squamosa* in our laboratory (Institute of Medicinal Plant Development [IMPLAD], Beijing, China). Paclitaxel (PTX) injections were supplied by Beijing Union Pharm Ltd. (Beijing, China). Monomethoxyl [poly (ethylene glycol)2000] -b- [poly (ε-caprolactone)2000] ($mPEG_{2k}$-PCL_{2k}) was purchased from JiNan Daigang Biotech Co., Ltd. (Jinan, China).20(S)-ginsenoside Rh2 (purity>98%) was obtained from Nanjing Spring & Autumn Biotech Co., Ltd. (Nanjing, China). Oleic acid (OA), Resiquimod (R848) was obtained from Shanghai Macklin Biochemical Co., Ltd. (Shanghai, China). IR780 was purchased from Sigma Aldrich (St. Louis, MO, USA). RPMI 1640 medium, DMEM medium, fetal bovine serum, 0.25% pancreatase, penicillin and streptomycin were obtained from Gibco (Grand Land, USA). Phosphate-buffered saline (PBS) was purchased from HyClone Biochemical Products Co., Ltd. (IL, USA). All other reagents were of analytical grade or higher. Deionized water was used in the experiments.

Cell Lines and Animals

The 4T1 cell lines, 293T and RAW 264.7 cells were obtained from the China Infrastructure of Cell Line Resources. The 4T1 cell cultured in RPMI 1640 medium, 293T and RAW 264.7 cells were cultured in DMEM medium at 37 °C with 5% CO_2 (Termo311, Waltham, MA, USA). The media were supplemented with 10% fetal calf serum and 100 U/mL penicillin and streptomycin (Gibco, St Louis, MO, USA).

Female BALB/c mice (20 ± 2 g, 6 – 8 weeks old) and male C57BL/6 mice (20 ± 2 g, 6 – 8 weeks old) were provided by Vital River Laboratory Animal Technology Co., Ltd. (Beijing, China). All mice were kept under the 12 h light–dark cycle environment with a relative humidity of 70 ± 5% at 25°C. All animal experiments were conducted in accordance with the Guidelines for Ethical and Regulatory for Animal Experiments as defined by the Institute of Medicinal Plant Development (IMPLAD), China. Ethical approval for this study was granted by the ethics committee of IMPLAD.

Preparation and Characterization of Nanoparticles

The antisolvent precipitation method was adopted to prepare the drug-loaded NPs. Briefly, a mixture of squamocin (Squ), Rh2, IR780, $mPEG_{2k}$-PCL_{2k}, and OA at a weight ratio of 1:100:25:100:300 was co-dissolved in a mixture of 1 mL methanol and 1 mL acetone and then slowly dropped into deionized water under ultrasonication (250 W, 25 °C ± 2 °C, Kunshan Ultrasonic Instruments Co., Ltd, Kunshan, PR China). The organic solvent was removed by evaporation under reduced pressure at 45 °C to obtain Squ-Rh2-IR780 NPs. When Rh2 or IR780 was absent in the formulation, the same procedure as above was used to obtain the Squ-IR780 NPs and Squ-Rh2 NPs. Squ-R848-IR780 NPs were also fabricated according to the above procedure at a weight ratio of 1: 50: 25: 100: 300 (Squ: R848: IR780: $mPEG_{2k}$-PCL_{2k}: OA).

A dynamic light scattering (DLS) instrument (Zetasizer Nano ZS, Malvern Instruments, UK) was used to detect the mean particle size, polydispersity index (PDI), and zeta potential of all of the above nanoparticles at 25 °C. Each measurement was performed in triplicate with 10 runs.

The morphology of the Squ-Rh2-IR780 NPs and Squ-R848-IR780 NPs was observed by transmission electron microscopy (TEM, JEM-1200, Tokyo, Japan). Briefly, 10.0 μL of water-diluted NPs was dropped on a 300-mesh copper net, allowed to stand for 10 min, stained with 2% (w/v) phosphotungstic acid hydrate liquid for 1 min, air dried, and then observed under TEM at an accelerating voltage of 80 kV.

Four milliliters of the freshly prepared nanoparticles were accurately weighed and lyophilized, and the lyophilized powder was dissolved in 40 mL of methanol and centrifuged at 13,000 rpm for 10 min. The supernatant was analyzed for the total concentration of Squ, Rh2 or R848 by high-performance liquid chromatography (HPLC) to calculate the drug

content of each drug in the lyophilized powder. Another 4 mL of NPs was put into an ultracentrifugation filter (5 mL, NMWL 3K, Millipore, USA) and centrifuged at 13,000 rpm for 20 min (4°C). The filtrate was diluted to 10 mL with methanol, and the concentrations of free Squ, free Rh2 and free R848 were measured.

In addition, the IR780 content of the above samples was determined at 780 nm using a UV–VIS spectrophotometer. The full wavelength scan of IR780 is shown in Figure S1. UV spectrophotometry and chromatographic conditions are detailed in the Supplementary Information. Drug loading capacity (DLC) (Eq. 1.) and encapsulation efficiency (EE) (Eq2.) were calculated as follows:

$$DLC(\%) = \frac{C_{total} \times V1}{W_{NPs}} \times 100\% \quad (1)$$

$$EE(\%) = \frac{C_{total \times V1} - C_{free} \times V2}{C_{total} \times V1} \times 100\% \quad (2)$$

where C_{total} is the concentration of each drug in the NPs, V1 is 40 mL, W_{NPs} is the weight of the lyophilized powder, C_{free} is the concentration of each free drug, and V2 is 10 mL.

The Stability of NPs in Physiological Media

The freshly prepared NPs were mixed with the same volume of 1.8% NaCl solution and 10% glucose solution or mixed with four volumes of PBS and mouse plasma, followed by incubation at 37 °C. The particle size and polydispersity index of the mixture were measured at different time intervals, and the possible physical changes, such as turbidity and precipitation, were also monitored to examine the stability of NPs in physiological media. Each experiment was performed in triplicate. In addition, the nanoparticles were kept at 4 °C, and their particle size was tested every week.

In vitro Photothermal Conversion Effect

We first evaluated the photothermal performance of IR780-containing NPs by real-time monitoring of their temperature change during a 5-minute period of laser irradiation. Squ-Rh2-IR780 NPs with IR780 concentrations of 10, 50, 100, 200, and 250 μg/mL was irradiated with 808 nm laser irradiation (WuHan Laserlan Co., Ltd. China, Wuhan) at a power density of 1.0 W/cm^2 for 5 min. Meanwhile, pure water, IR780 methanol solution and various nanoformulations containing 250 μg/mL IR780 were also irradiated using an 808 nm laser for 5 min. During irradiation, the temperature variation in each sample was recorded using a Variocam HD Research Portable Thermal Energy Ecological Research System (InfraTec GmbH Infrarotsensorik und Messtechnik, Dresden, Germany).

Additionally, the photothermal capacity of Squ-Rh2-IR780 NPs, Squ-R848-IR780 NPs and free IR780 after multiple irradiation was also measured at different times. Subsequently, the photothermal conversion efficiency of IR780-containing formulations and free IR780 was calculated according to the reference[29] (see the detailed methods in the supplementary information). To evaluate the photothermal stability of Squ-Rh2-IR780 NPs and Squ-R848-IR780 NPs, we further detected their temperature-rising profile during 3 cycles of laser on/off irradiation at a power density of 1.0 W/cm^2.

In vitro Cytotoxicity Assay

Murine breast cancer 4T1 /293T cells in the logarithmic phase were seeded in 96-well plates (8000 cells/well) and incubated at 37 °C for 24 h with 5% CO_2. Then, the culture medium was replaced by a series of concentrations of free squamocin or squamocin-containing nanoformulations with blank medium as a negative control, followed by incubation for 72 h. Afterward, 20 μL MTT (5 mg/mL) (Sigma Aldrich, St. Louis, MO, USA) was added to each well and incubated for 4 h. Then, 200 μL DMSO was added and shaken for 20 min. The absorbance of the solution in each well was then measured using a plate reader (Biotek Synergy H1, VT, USA) at 490 nm. The cell survival rate was calculated according to the following formula:

$$\text{Cellular viability}(\%) = OD_n / OD_t * 100\% \quad (3)$$

where OD_t and OD_n are the mean optical densities of the treated group and negative control group, respectively. The 50% inhibitory concentration value (IC_{50}) was calculated using GraphPad Prism Software, Version 5 (GraphPad Software, Inc., La Jolla, CA, USA).

In vitro BMDC Maturity Assay

Immature BMDC were obtained according to the BMDC isolation protocol (Abcam, USA). Bone marrow cells were isolated from the femur and tibia of C57BL/6 mice (male, 6 – 8 weeks old). Bones were cut under aseptic condition, and the bone marrow cells were blown out with medium, filtered through a 70 μm cell strainer. Red blood cells are cleaved using red blood cell lysate, and then inoculated into 10 cm ultra-low attachment Petri dishes containing 10 mL of RPMI −1640 medium supplemented with 10% FBS and 20 ng/mL GM-CSF (Thermo Fisher, USA). Cells were cultured in a 37°C incubator containing 5% CO_2. Cells were harvested on the eighth day, then cells were treated with PBS, Squ-IR780 NPs, Squ-Rh2-IR780 NPs, Squ-R848-IR780 NPs, respectively for 48 hours, and irradiated with NIR 1W/cm^2 for 3 mins at the 6th h. Then the cells were centrifuged at 3500 r, 5 min, and the supernatant was collected to do the Elisa kit according to the producer's protocol, cells were added with Anti-CD86 antibody-FITC (0.2 μg/10^6 cells), Anti-MHC II antibody-APC (0.2 μg/10^6 cells) for 30 min (Elabscience, China), according to the producer's protocol, and analyzed using flow cytometry.

In vitro Repolarization Experiment

To assess the polarizing effect of multifunctional NPs on tumor associated macrophages (TAMs), RAW264.7 (10^5/well) was firstly stimulated by IL-4 (20 ng/mL, 2 mL) in vitro to generate M2-type macrophages. 24 h later, the supernatant was discarded, the cells were incubated with 2 mL of free R848, free Rh2, Squ-IR780 NPs, Squ-R848-IR780 NPs and Squ-Rh2-IR780 NPs respectively for 24 h with the equivalent dose of 20 μg/mL for R848 and 40 μg/mL for Rh2, followed by centrifuge at 3500 rpm for 5 min. The supernatant was collected for Elisa kit assay according to the producer's protocol, the collected cells were treated with anti-CD86-PE (0.2 μg / 10^6 cells), fixed with 4% paraformaldehyde, then the intracellular staining was performed with anti-CD206-FITC (0.1 μg / 10^6 cells), (Biolegend, SD, USA), and the macrophage phenotype was determined by flow cytometer using specific markers.

In vivo Biodistribution in 4T1 Tumor-Bearing Mice

The 4T1 tumor-bearing mouse model was established as described above. When the tumor volume reached approximately 1000 mm^3, the mice were randomly divided into 6 groups (n=3) and treated with Squ-IR780 NPs, Squ-Rh2-IR780 NPs, Squ-R848–IR780 NPs, Squ-IR780 NPs + laser, Squ-Rh2-IR780 NPs + laser, or Squ-R848–IR780 NPs + laser (0.1 mg/kg equivalent of Squ, 10 mg/kg equivalent of Rh2, 5 mg/kg equivalent of R848, and 2.5 mg/kg equivalent of IR780).

After a single dose of intravenous administration of the above nanoparticles, all of the mice were fluorescently imaged (IVIS Living Image VR version 4.4 three-dimensional optical in vivo imaging system for small animals, PerkinElmer Inc. NY, USA) at 0, 2, 4, 8, 12, 24, 36 and 48 h post dose (excitation wavelength 745 nm, emission wavelength 820 nm). At the 24th hour, the tumor region of the mice in the three specified groups (Squ-IR780 NPs +laser, Squ-Rh2-IR780 NPs + laser, Squ-R848–IR780 NPs +laser) was irradiated using an 808 nm laser at 1 W/cm^2. At the end of the experiment, the mice were sacrificed by cervical dislocation, and the tumor, heart, liver, spleen, lung, kidney, and brain were dissected and imaged as described above. The relative tumor targeting index (RTTI) was calculated according to Eq. (4):

$$RTTI\% = F_t/F_{lv} \times 100\% \quad (4)$$

where F_t, F_{lv}, F_h, F_s, F_{lu}, and F_k are the average fluorescence intensities in the mouse tumor, liver, heart, spleen, lung, and kidney, respectively.

In vivo Antitumor Efficacy in 4T1 Tumor-Bearing Mice

4T1 cells in logarithmic phase were suspended in RPMI medium without fetal calf serum, and 1.0×10^6 cells were subcutaneously inoculated into the right armpit of female BAL B/c mice to establish a 4T1 tumor-bearing mouse model. When the mean tumor volume reached approximately 200 mm^3, the mice were randomly divided into 10 groups (10 mice

each): the negative control group (normal saline), positive control group (PTX injection, 8 mg/kg), Squ NPs group, Squ-IR780 NPs, Squ-Rh2 NPs, Squ-R848 NPs, R848-IR780 NPs, Rh2-IR780 NPs, Squ-Rh2-IR780 NPs and Squ-R848-IR780 NPs (0.1 mg/kg Squ, 10 mg/kg Rh2, 5 mg/kg R848, 2.5 mg/kg IR780). The 10 groups of mice were injected intravenously every 3 days for 5 doses. The mice in the four groups dosed with IR780-containing nanoparticles were irradiated twice with an 808 nm NIR laser for 5 minutes (WuHan Laserlan Co., Ltd. China, Wuhan) (1 W/cm2) at the 24th and 48th hours after each dose. Meanwhile, the local tumor temperature was monitored using an IR thermal imaging camera (InfraTec GmbH Infrarotsensorik und Messtechnik, Dresden, Germany) during irradiation. Tumor volume (calculated according to Eq. (5)) and body weight were measured every 3 days for all of the mice. At 48 hours after the last dose, 3 mice in each group were randomly selected and sacrificed according to the institutional guidelines, the tumors were dissected and weighed, and the tumor inhibition rate (TIR) was calculated according to Eq. (6). Serum IFN-γ (Dogesce Beijing, China) was determined by a microplate reader (Rayto RT-6100, Shenzhen Raydu Life Science Co., LTD. China, Shenzhen). Major organs, such as the liver, spleen, lung, kidney and thymus, were collected, weighed, fixed, sliced and cut with paraffin. The liver, spleen and thymus indexes were calculated by Eq. (7–9). The sections were stained with hematoxylin and eosin (H&E) for histological analysis. The lung tissue was fixed with Bouin solution for 24 hours and rinsed with anhydrous ethanol to yellow. The tumor metastases in the lung were observed under a microscope, and the number of lung metastatic nodules was counted by a single blind method to calculate the pulmonary metastasis inhibition rate (PMIR) (Eq 10).

$$V\left(mm^3\right) = 0.5 \times \ ab^2\left(mm^3\right) \tag{5}$$

$$TIR(\%) = \left(1 - \frac{W_t}{W_n}\right) \times 100\% \tag{6}$$

$$\text{Liver index} = \frac{W_{LI}}{W} * 100\% \tag{7}$$

$$\text{Spleen index} = \frac{W_{SP}}{W} * 100\% \tag{8}$$

$$\text{Thymus index}(\%) = \frac{W_{TH}}{W} * 100\% \tag{9}$$

$$PMIR(\%) = \frac{N_m - N_n}{N_m} \times 100\% \tag{10}$$

where a is the longest diameter of the tumor, b is the shortest diameter of the tumor, and W_t and W_n are the mean tumor weights of the treated group and negative control group, respectively. W_{LI}, W_{SP}, W_{TH}, W are the weights of the liver, spleen, thymus and body weight, respectively. N_n and N_m are the mean number of pulmonary nodules in the treated group and negative control group, respectively.

The remaining 7 mice in each group were normally fed for continuous observation, and their body weight and tumor volume were regularly measured. Mice with a tumor volume greater than 2000 mm³ were considered dead and euthanized.

Results and Discussion

Preparation and Characterization of Nanoparticles

In this study, both Squ-Rh2-IR780 NPs and Squ-R848-IR780 NPs were prepared for the comparative in vitro and in vivo study. Thus, it is best to use the same pharmaceutic excipients and the same procedure to fabricate the two NPs, which is not easy due to that three active pharmaceutic ingredients (APIs) need to be encapsulated into the same NPs. After repeated attempts, it was found that the addition of oleic acid (OA) was conducive to encapsulate the three APIs in the same nanoparticle, and the current prescription was finally screened by taking particle size and stability as screening

indexes. Meanwhile the liquid property of OA may confer the OA-containing nanoparticles with certain elasticity and thus may help the NPs to be delivered to tumor, as reported in our previous study.[30]

The resultant Squ-Rh2-IR780 NPs and Squ-R848-IR780 NPs showed average particle sizes of (162.200 ± 2.800) nm and (157.300 ± 1.1590) nm, respectively, with PDI values of 0.190 ± 0.017 and 0.120 ± 0.009, when they scattered across PBS, their surface zeta potentials were (−5.120 ± 0.411) mV and (−8.590 ± 1.060) mV (Figure 2A and B), and neutral and weakly negative charges can help NPs escape serum protein adsorption. TEM observation demonstrated that both NPs were spherical with some small spines on their surfaces (Figure 2C and D), which was unusually observed. The encapsulation efficiencies of Squ, R848, Rh2 and IR780 were all over 85% in all of the NPs (Table S1). Among them, the encapsulation efficiency of Squ-Rh2-IR780 NPs for Rh2 and IR780 can reach (88.02 ± 0.77) % and (86.04 ± 0.02) % respectively, and the encapsulation efficiency of Squ-R848-IR780 NPs for R848 and IR780 can reach (90.70 ± 1.00) % and (86.13 ± 0.028) % respectively. Based on the definition of drug loading, NPs with drug loading more than 10% are usually defined as high drug loading NPs,[31] and the drug loading of multifunctional NPs for total drugs is more than 10%, and the actual drug loading content was close to the theoretical value (Tables S2–S4), indicating the good compatibility of these NPs for various types of hydrophobic drugs.

Stability in Physiological Media and on-Shelf

Here, the stability of Squ-Rh2-IR780 and Squ-R848-IR780 NPs in physiological media and in plasma was investigated. As seen in Figure 3A and B, both Squ-Rh2-IR780 and Squ-R848-IR780 were quite stable in normal saline, 5% glucose, PBS, or plasma with limited particle size and PDI changes, which demonstrates their suitability for intravenous injection. During the 5 weeks of storage at 4°C, both NPs displayed insignificant particle size and PDI changes (Figure 3C and D). The mean particle size and PDI change profiles of Squ NPs, Squ-IR780 NPs, Squ-Rh2 NPs, Squ-R848 NPs, Rh2-IR780 NPs and R848-IR780 NPs in physiological media are shown in Figure S2A–F, indicating their presentable stability.

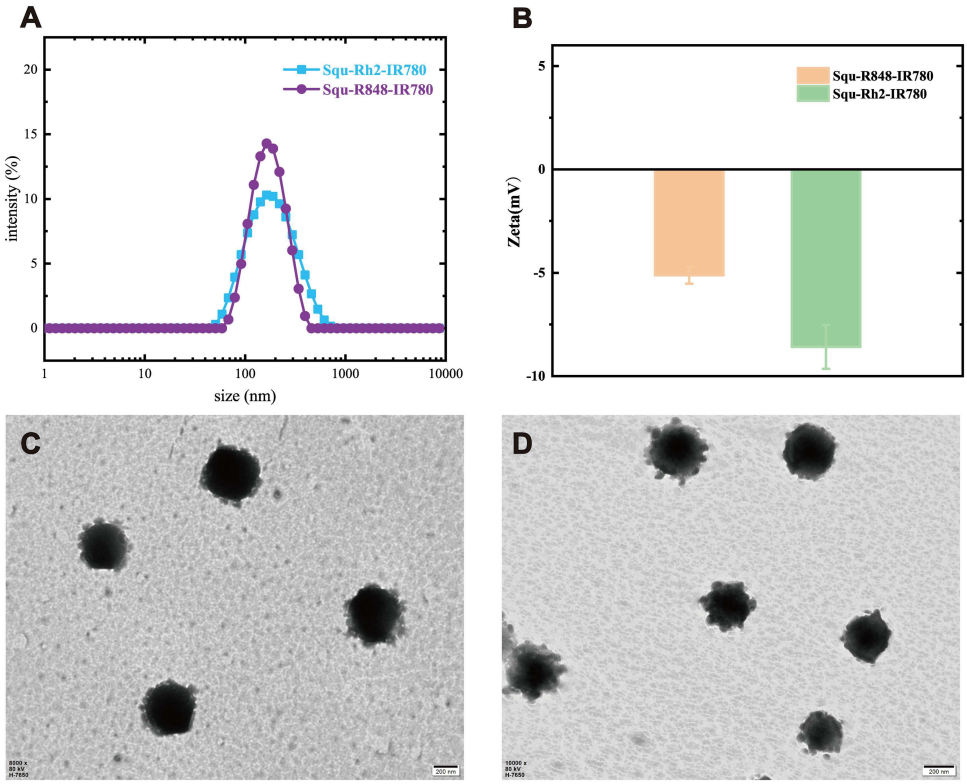

Figure 2 Characterization of the Squ-Rh2-IR780 NPs and Squ-R848-IR780 NPs. The particle size distribution (**A**), and zeta potential (**B**) of Squ-Rh2-IR780 NPs and Squ-R848-IR780 NPs, error bars are based on SD (n=3). The TEM morphology of Squ-Rh2-IR780 NPs. (**C**) and Squ-R848-IR780 NPs (**D**).

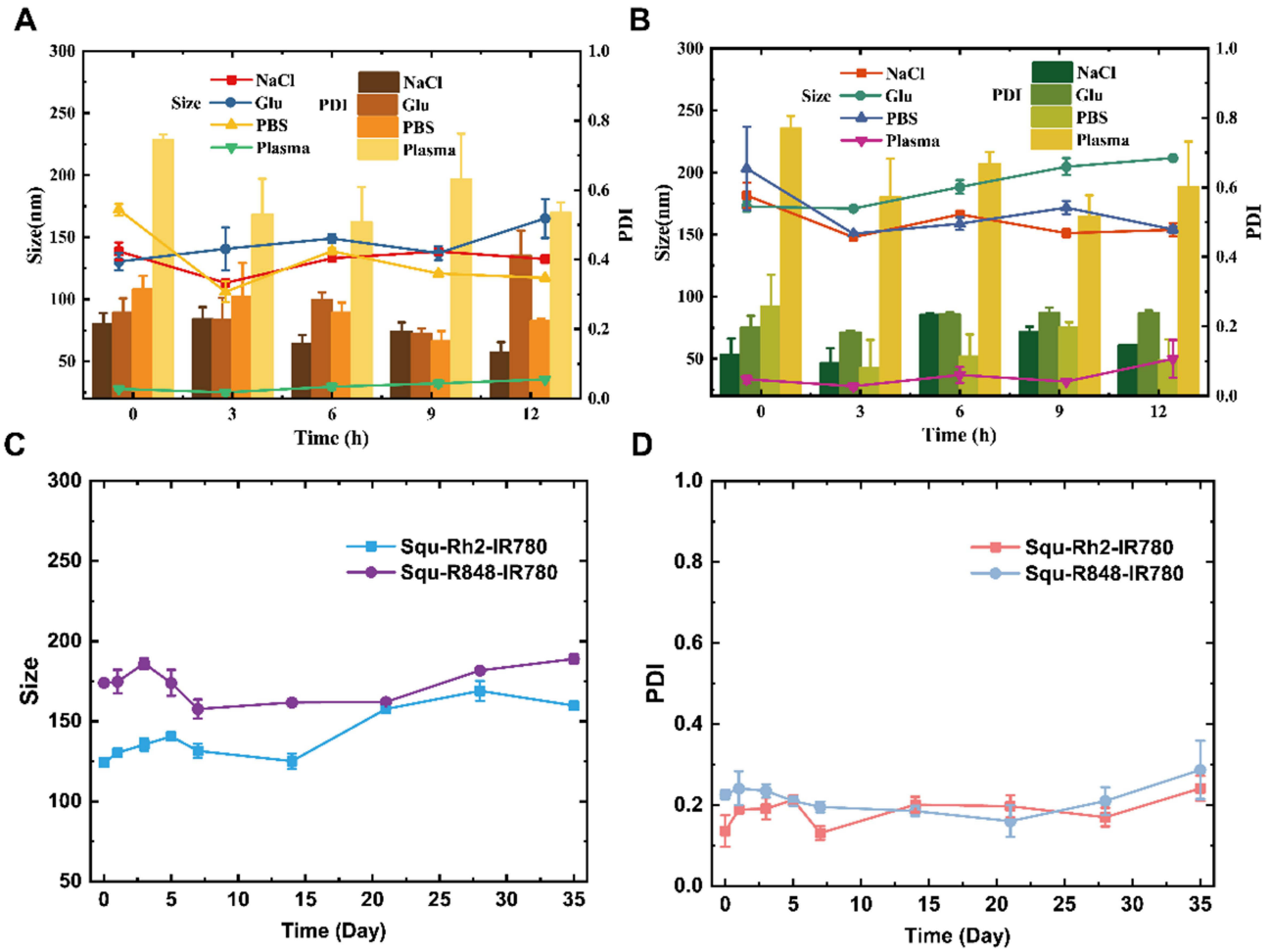

Figure 3 The stability of the Squ-Rh2-IR780 and Squ-R848-IR780 NPs. The mean particle size and PDI change of Squ-Rh2-IR780 (**A**) and Squ-R848-IR780 NPs (**B**) in physiological media. The mean particle size (**C**) and PDI (**D**) change of Squ-Rh2-IR780 NPs and Squ-R848-IR780 NPs at 4°C storage.

In vitro Photothermal Conversion Effect

During exposure to the 808 nm laser, the IR780 solution showed a concentration- and time-dependent temperature rise (Figure 4A). After 808 nm irradiation for 5 minutes, pure water showed little temperature rise; however, IR780-containing NP formulations, including Squ-IR780 NPs, R848-IR780 NPs, Rh2-IR780 NPs, Squ-R848-IR780 NPs, and Squ-Rh2-IR780 NPs (all at a concentration of 250 μg/mL of IR780), displayed much higher elevated temperatures (from 25°C to nearly 60°C) (Figure 4B and C). During the 3 successive cycles of laser on/off irradiation, Squ-Rh2-IR780 NPs, Squ-R848-IR780 NPs and IR780/methanol solution displayed the same temperature change without any attenuation (Figure 4D), indicating that Squ-R848-IR780 NPs and Squ-Rh2-IR780 NPs had outstanding photothermal performance and could be used as promising PTT agents for cancer ablation. Linear time data versus –ln (θ) obtained from the cooling period of Squ-Rh2-IR780 NPs and Squ-R848-IR780 NPs are shown in Figure S3A and B. The photothermal conversion efficiency (PCE, η) of the two multifunctional NPs was determined using a previously reported method[32,33] to be approximately 24.10% and 22.58%, which was in accordance with the most reported values of the heptamethine cyanine dyes (PCE ≈ 3–20%).[34]

In vitro Cytotoxicity Assay

The in vitro cytotoxicity of free Squ and Squ-containing NPs against 4T1 cells was investigated by MTT assay. As shown in Figure S4A–J, the viability of 4T1 cells was dose-dependent for free Squ solution and Squ-containing NPs, and there was no obvious toxicity to 293T for Squ-containing preparation. Free Squ and Squ NPs displayed very strong cytotoxicity against

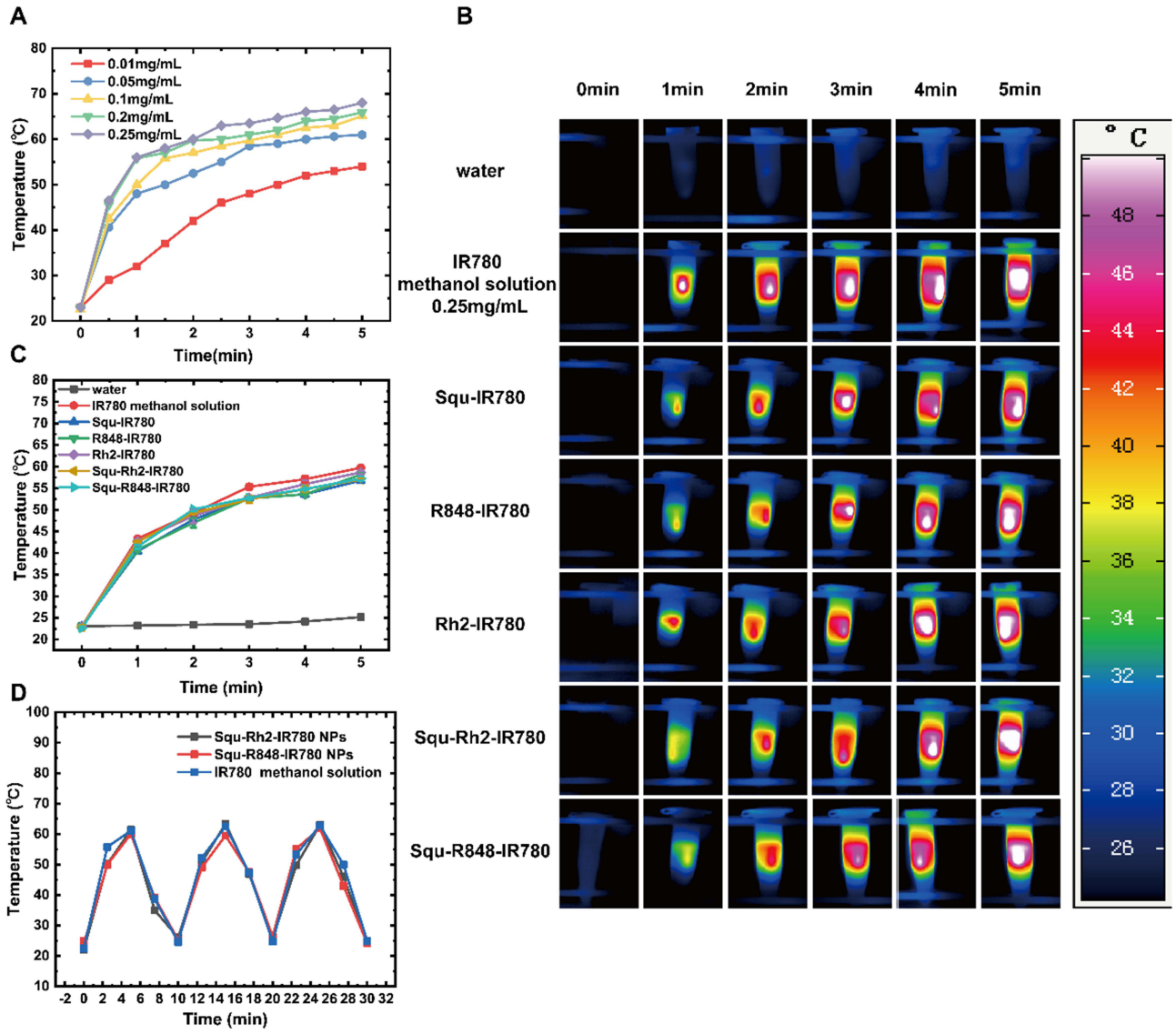

Figure 4 In vitro photothermal conversion effect of Squ-Rh2-IR780 NPs and Squ-R848-IR780 NPs. (**A**) Temperature change of different concentrations of IR780 methanol solution during irradiation with an 808 nm laser. (**B**) Infrared thermal images of photothermal NPs at a concentration of 0.25 mg/mL under 808 nm laser irradiation at different power densities (1.0 W/ cm^2). (**C**) Temperature change of Squ-Rh2-IR780 NPs, Squ-R848-IR780 NPs and IR780 methanol solution (containing 0.25 mg/mL IR780) during 3 successive cycles of laser on/off irradiation. (**D**) Temperature change of different NPs (containing 0.25 mg/mL equivalent IR780) during irradiation, using pure water and 0.25 mg/mL IR780/methanol solution as a control.

4T1 cells, with IC_{50} values of (0.460 ± 0.014) μg/mL and (0.444 ± 0.014) μg/mL, respectively (Figure 5). However, R848 and Rh2 showed much lower toxicity against 4T1 cells (Figure S4K), which is consistent with the reported data.[35] The co-loading of R848, IR780 or Rh2 enhanced the cytotoxicity of the Squ NPs by 1.05-fold, 1.72-fold and 9.05-fold, respectively. Triple coloaded Squ-R848-IR780 NPs displayed an IC_{50} value of 0.0626 μg/mL, and Squ-Rh2-IR780 NPs displayed an IC_{50} value of 0.0074 μg/mL, with 6.01-fold and 59-fold enhanced cytotoxicity against 4T1 cells. With the help of NIR irradiation, the corresponding IC_{50} values further decreased to 0.020 μg/mL and 0.0014 μg/mL, indicating 21.21-fold and 316.28-fold cytotoxicity enhancement, respectively. The above in vitro data demonstrated strong synergistic effects of chemotherapy, immunoregulation and thermal therapy. Simply judging according to the in vitro data alone, ginsenoside Rh2 was superior to R848 in combination with Squ, IR780, and IR780+laser for tumor inhibition.

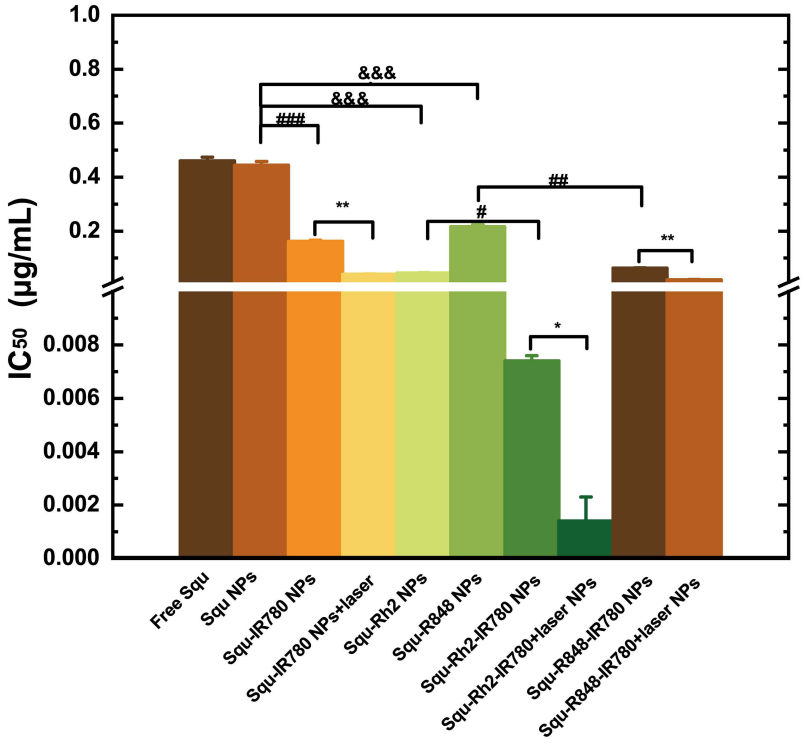

Figure 5 IC_{50} values for different groups of treated 4T1 cells (n=6). #Represents a significant difference between IR780 (+) and IR780 (-) (#$p<0.05$; ##$p<0.01$ ####$p<0.01$). *Represents a significant difference between the NPs + laser (+) and NPs +laser (-) (*$p<0.05$; **$p<0.01$). &Represents a significant difference between Rh2 (+) and Rh2 (-) or between R848 (+) and R848 (-) (&&&$p<0.001$). In vivo biodistribution in 4T1 tumor-bearing mice.

In vitro BMDC Maturity Assay

Mononuclear phagocytes, consisting of monocytes, macrophages and DCs, play a role in intrinsic immunity through pathogen sensing and phagocytosis, and act as interacting cellular components to present antigens to T cells in adaptive immunity. Among them, DCs are key antigen-presenting cells (APCs). Chemotherapeutic agents can cause apoptosis of tumor cells, release tumor associated antigen and DAMPs to induce the maturation of DCs, the most important APCs and play an immunomodulatory role to activate anti-tumor immunity and effectively improve the tumor immune microenvironment. R848, as a TLR7/8 agonist, can also induce the maturation of DCs, and the photothermal immuno-chemotherapeutic combination therapy system, as investigated herein, consists of immunotherapeutic molecules R848 or Rh2, photosensitizer IR780, and chemotherapeutic drug Squamocin. Squamocin acts directly on tumor cells and produces tumor debris, which, together with adjuvants R848 or Rh2, is used to stimulate maturation of APCs and polarization of macrophages toward the M1 phenotype. Here, the expression of activation markers $CD86^+$ and MHC-II on the surface of BMDCs was analyzed by flow cytometry to assess DCs maturity. Figure 6A and B show that the expression of these surface markers was significantly increased in Squ-R848-IR780 NPs and Squ-Rh2-IR780 NPs-treated BMDCs, and their proportion of $CD86^+$ MHC-II was significantly higher than that in BMDCs treated with Squ-IR780 NPs, which was accompanied by an increase in the expression of the cytokines TNF-α, IL-12 and IL-6 (Figure 6C–E) suggesting that immune adjuvant R848 and Rh2 induce DCs maturation.

In vitro Repolarization Experiment

Tumor microenvironment (TME) has attracted extensive attention due to its key role in regulating tumor cell survival and pathological development. In this process, TAMs are the main components of tumor-associated stromal cells, which can cause tumor-associated inflammation. M2-type of TAMs are the most abundant invasive immunosuppressive cells in tumors, which can promote tumor cell growth and participate in tumor invasion and metastasis by secreting a variety of immunosuppressive mediators. It was supposed that R848/Rh2 could promote the transformation of polarized M 2-type TAMs into M l- type, then enhance the tumor-killing function of macrophages. As shown in Figure 7A, RAW264.7 cells treated with free R848, free Rh2, Squ-R848-IR780 NPs + laser or Squ-Rh2-IR780 NPs + laser all displayed the

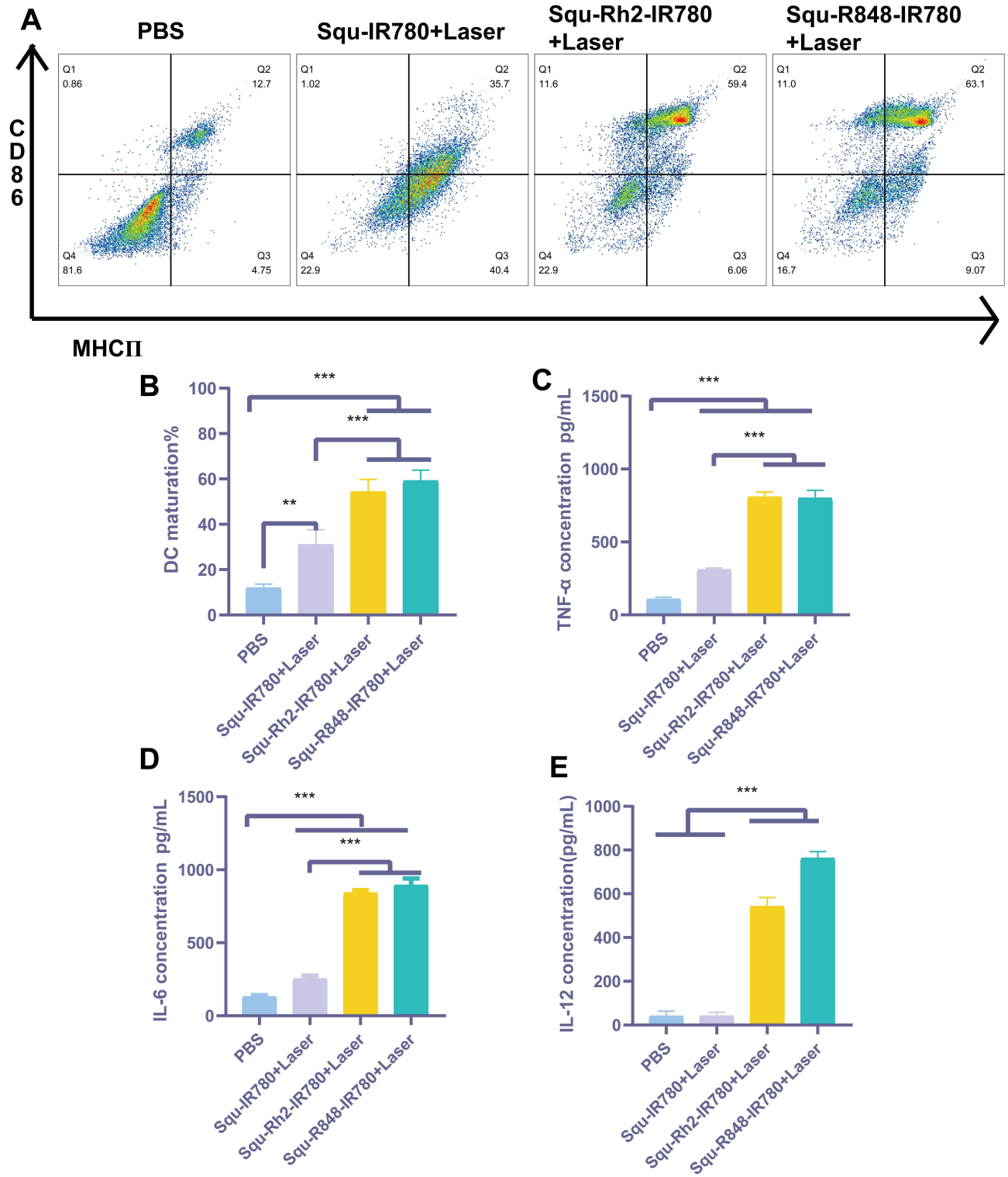

Figure 6 Squ-IR780 NPs, Squ-Rh2-IR780 NPs, Squ-R848-IR780 NPs groups increased DCs maturation. (**A** and **B**) for the flow cytometry analysis and the corresponding quantification of DCs surface activation markers. (**C**–**E**) for the Cytokine levels such as TNF-α(**C**), IL-6 (**D**) and IL-12 (**E**) secreted by DCs during maturation (n=3), the samples were tested by *t*-test, ***p*<0.01, ****p*<0.001.

significantly decreased CD206 expression and significantly increased CD86 expression in contrast to PBS and Squ-IR780 NPs, indicating of the successful transformation of M2 macrophages to M1 macrophages (Figure 7B) by R848 or Rh2, which was also evidenced by the increased levels of pro-inflammatory cytokines TNF-α and IL-6 (Figure 7C and D).

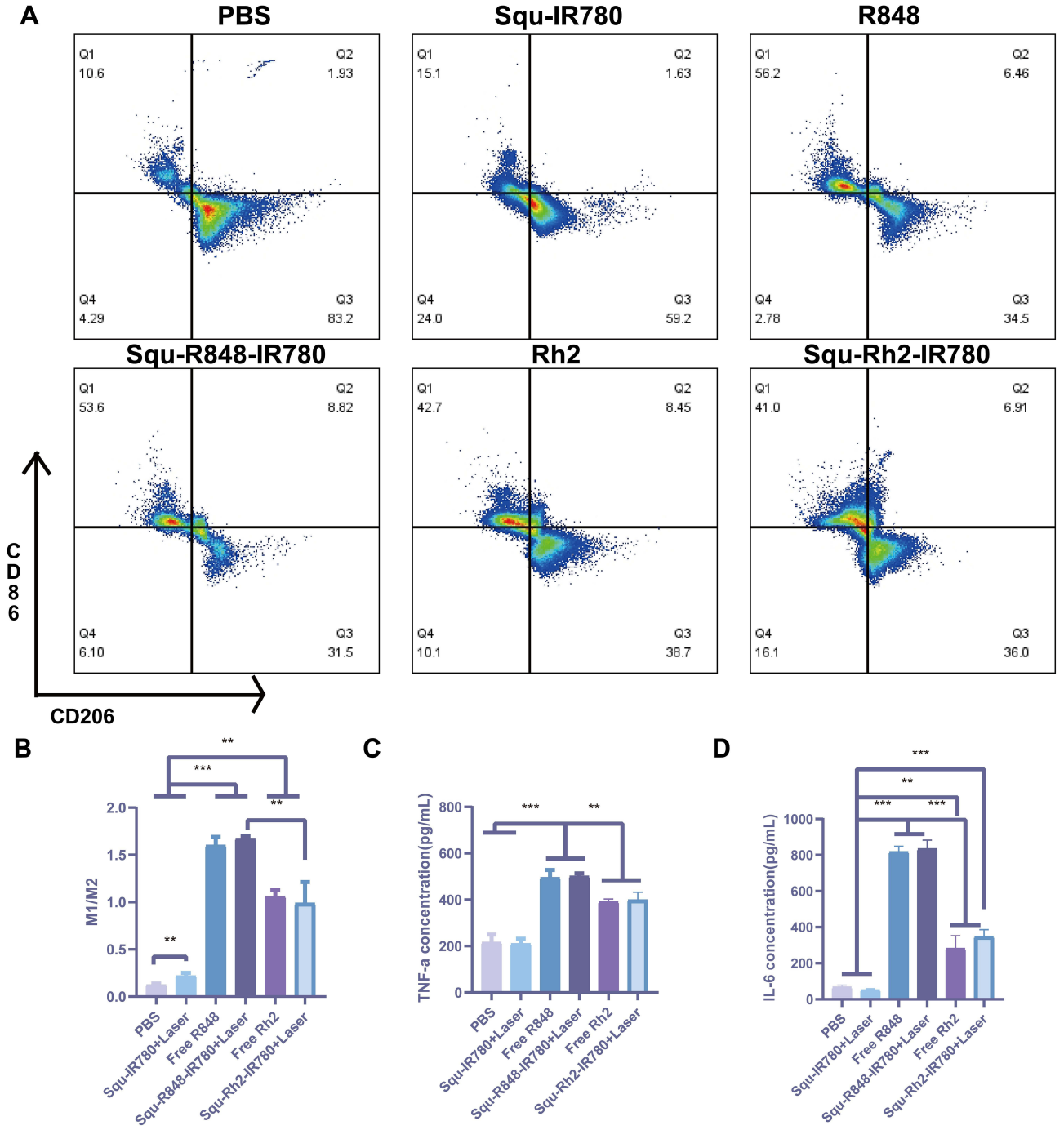

Figure 7 Flow cytometry analysis and corresponding quantification of M2-M1 macrophage surface activation markers. (**A** and **B**) for the flow cytometry analysis and corresponding quantification of M1 and M2 of RAW264.7 surface activation markers. TNF-α (**C**) and IL-6 (**D**) levels induced by PBS, Squ-IR780 NPs, R848, Rh2, Squ-R848-IR780 NPs, Squ-Rh2-IR780 NPs (n=3), $^{**}p<0.01$, $^{***}p<0.001$.

In vivo Biodistribution in 4T1 Tumor-Bearing Mice

As seen in the dynamic imaging data (Figure 8A), all of the tested NPs displayed very good tumor targetability. Obvious tumor accumulation was observed as early as the 4th hour, followed by a continuous enhancement of fluorescence in the tumor over time. In this regard, there was no significant difference among the three tested nanoparticles, Squ-IR780 NPs, Squ-Rh2-IR780 NPs and Squ-R848-IR780 NPs, except for slightly faster tumor accumulation in the Squ-IR780 NP group. At the end of the experiment, the direct fluorescent imaging of the dissected organs and tumors more clearly

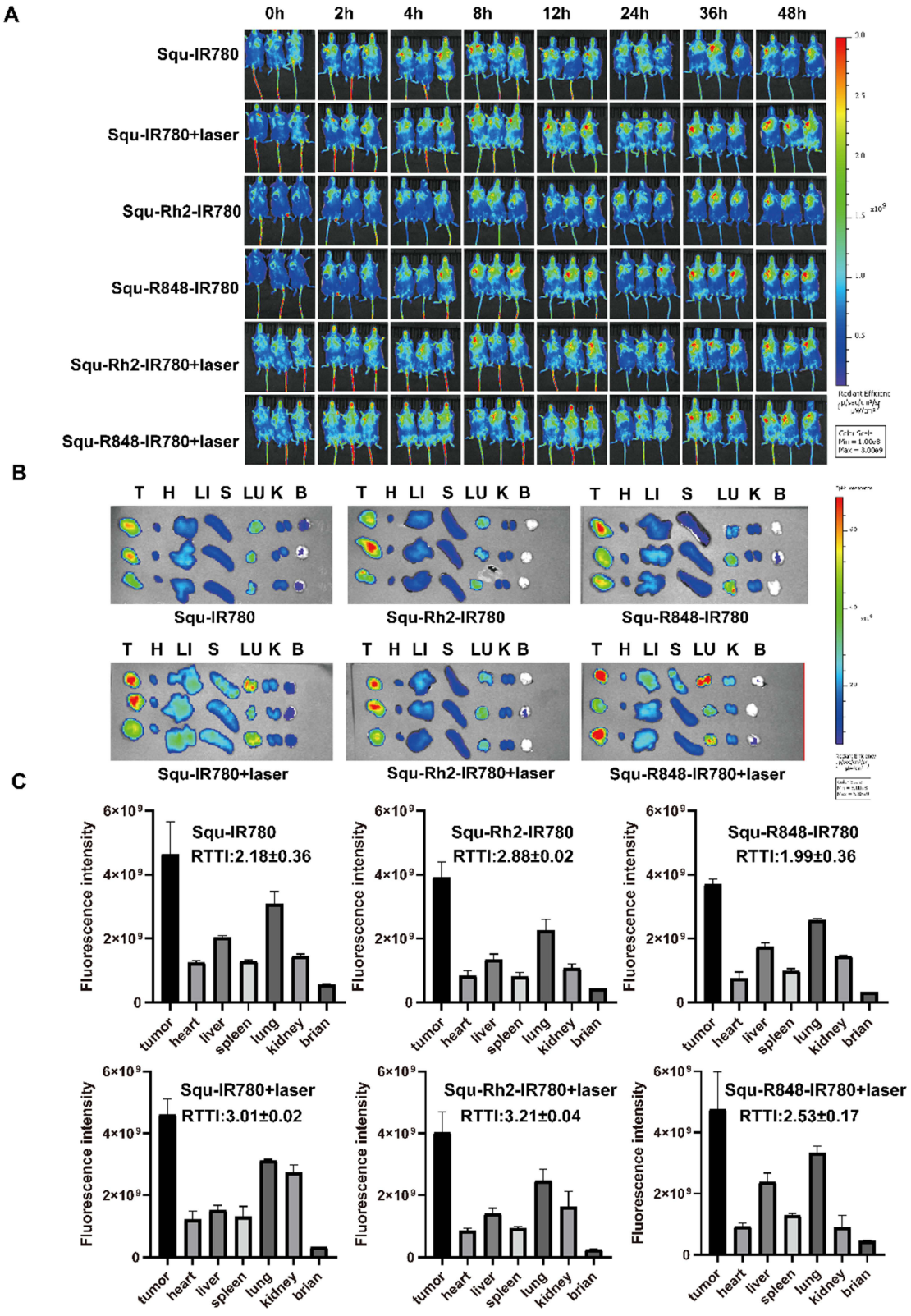

Figure 8 In vivo biodistribution in 4T1 tumor-bearing mice. (**A**) In vivo fluorescence images of mice at different times after intravenous injections of Squ-IR780, Squ-Rh2-IR780 NPs and Squ-R848-IR780 NPs with laser. (**B**) Ex vivo fluorescence image. T means tumor, H means heart, LI means liver, S means spleen, LU means lung, K means kidney, B means brain (**C**) Semiquantitative fluorescence analysis of each group of nanoparticles containing IR780 in vitro.

https://doi.org/10.2147/IJN.S448860 DovePress

demonstrated that the three fluorescently labeled nanoparticles were mainly distributed in tumors and then in the lungs, both significantly higher than in other organs (Figure 8B).

It was clear that 808 nm laser irradiation at the 24th hour post dose enhanced the subsequent (the 36th and 48th hour) tumor accumulation of NPs (Figure 8A and B). The semiquantitative analysis of fluorescence (Figure 8C and Table S5) also clearly showed that additional NIR irradiation in the tumor region could significantly promote the relative tumor targeting index (RTTI) of Squ-IR780 NPs (3.01±0.02 vs 2.18±0.36, $p<0.05$), Squ-Rh2-IR780 NPs (3.21±0.04 vs 2.88 ±0.02, $p<0.01$) and Squ-R848-IR780 NPs (2.53±0.17 vs 1.99±0.36, $p<0.05$). This was because the photothermal effect of the IR780-containing nanoparticles that had accumulated in the tumor increased the local tumor temperature, which then could enhance the permeability of tumor blood vessels and reduce the tumor interstitial pressure.[36,37] Recently, it was reported that, in addition to the endothelial barrier, the tumor vascular basement membrane surrounding the endothelium entraps NPs in the subendothelial void, forming perivascular NP pools and acting as a formidable mechanical barrier seriously hampering the delivery of nanotherapeutics to tumors.[38] Coincidentally, local hyperthermia can trigger acute sterile inflammation in the tumor region and recruit leukocytes locally to the NP pools, triggering NP pool eruptions into the tumor interstitium, resulting in increased NP penetration into deeper tumors.[39] Thus, the photothermal effect could be a very promising strategy to enhance tumor-targetability of nanoparticles in multiple ways.

In vivo Antitumor Efficacy and Photothermal Efficacy in 4T1 Tumor-Bearing Mice

To verify whether the two multifunctional NPs could achieve the synergistic effect of chemotherapy, immune regulation and photothermal therapy, thus yielding a marked antitumor therapeutic efficacy, 9 groups of 4T1 tumor-bearing mice were investigated with the administration regime shown in Figure 9A.

As seen in Figures 9B and 10A, the tumors of the normal saline group grew very quickly, while PTX injection (Figure 10B) treatment at a dose of 8 mg/kg significantly slowed tumor growth ($p<0.05$), with a tumor inhibition rate (TIR) of 43.64% (Table S6). The Squ NPs group at a dose of 0.1 mg/kg displayed a further smaller tumor ($p<0.05$) and a higher TIR of 55.28% (Figure 10C). Considering the much lower dose of Squ than that of PTX, it was clear that Squ was a potent chemotherapeutic agent. Regardless of IR 780 (Figure 10D), Rh2 (Figure 10E) or R848 (Figure 10F), the combined use with Squ obtained a significant antitumor efficacy, with the TIR being 69.30% ($p<0.05$, contrast to Squ NPs), 76.74% ($p<0.01$), and 74.39% ($p<0.01$), demonstrating the strong synergistic effect of Squ chemotherapy and immunoregulation.

Neither Rh2 nor R848 had strong cytotoxicity against 4T1 cells in vitro (Figure S4B). Interestingly, in the absence of chemotherapeutic agents (Squ), Rh2-IR780 NPs (Figure 10G) and R848-IR780 NPs (Figure 10H) displayed presentable in vivo antitumor efficacy, with TIRs of 51.64% and 54.65%, respectively, which were close to the TIR of Squ alone (55.28%). This was because under 808 nm laser irradiation, all mice treated with IR780-containing NPs displayed a rapid increase in tumor temperature to approximately 45 °C within 3 min and approximately 48 °C within 5 min (Figure S5A and B), which led to good photothermal therapy. Mild hyperthermia (39–42 °C) at tumors promotes perfusion, dilates blood vessels and enhances oxygenation,[40] thereby sensitizing tumors to chemo- and radiotherapy.[41,42] Local hyperthermia therapy (>42°C) can induce tumor cell apoptosis without causing damage to other organs, or burns to mice.[43–45]

However, when the chemo-, immuno- and photothermal therapies were combined, the Squ-Rh2-IR780 NPs (Figure 10I) and Squ-R848-IR780 NPs achieved markedly enhanced therapeutic efficacy, with TIR values of 91.42% and 95.65%, respectively. Especially for the Squ-R848-IR780 group, the primary tumors in 2 of 10 mice were completely ablated without any evidence of recurrence during the subsequent observation period (Figures 9C and 10J). The TIR data calculated by tumor weight from 3 mice in each group sacrificed on the 20th day were in accordance with the TIR data calculated by the tumor volume.

Cytokine secretion is a typical indicator of the immune response. All groups treated with Rh2- or R848-containing nanoparticles showed significantly enhanced serum IFN-γ concentrations, especially for Squ-Rh2 NPs, Squ-Rh2-IR780 NPs and Squ-R848-IR780 NPs ($p<0.01$, in contrast to the normal saline group) (Figure 9D). It was reported that potent chemotherapy or photothermal therapy could induce tumor cell apoptosis and the release of tumor-associated antigens. Immunomodulators such as R848 and Rh2 can trigger DCs maturation and antigen presentation, thus activating the immune response to further kill tumor cells or inhibit tumor cell growth. As an agonist of TLR 7/8, R848 triggers

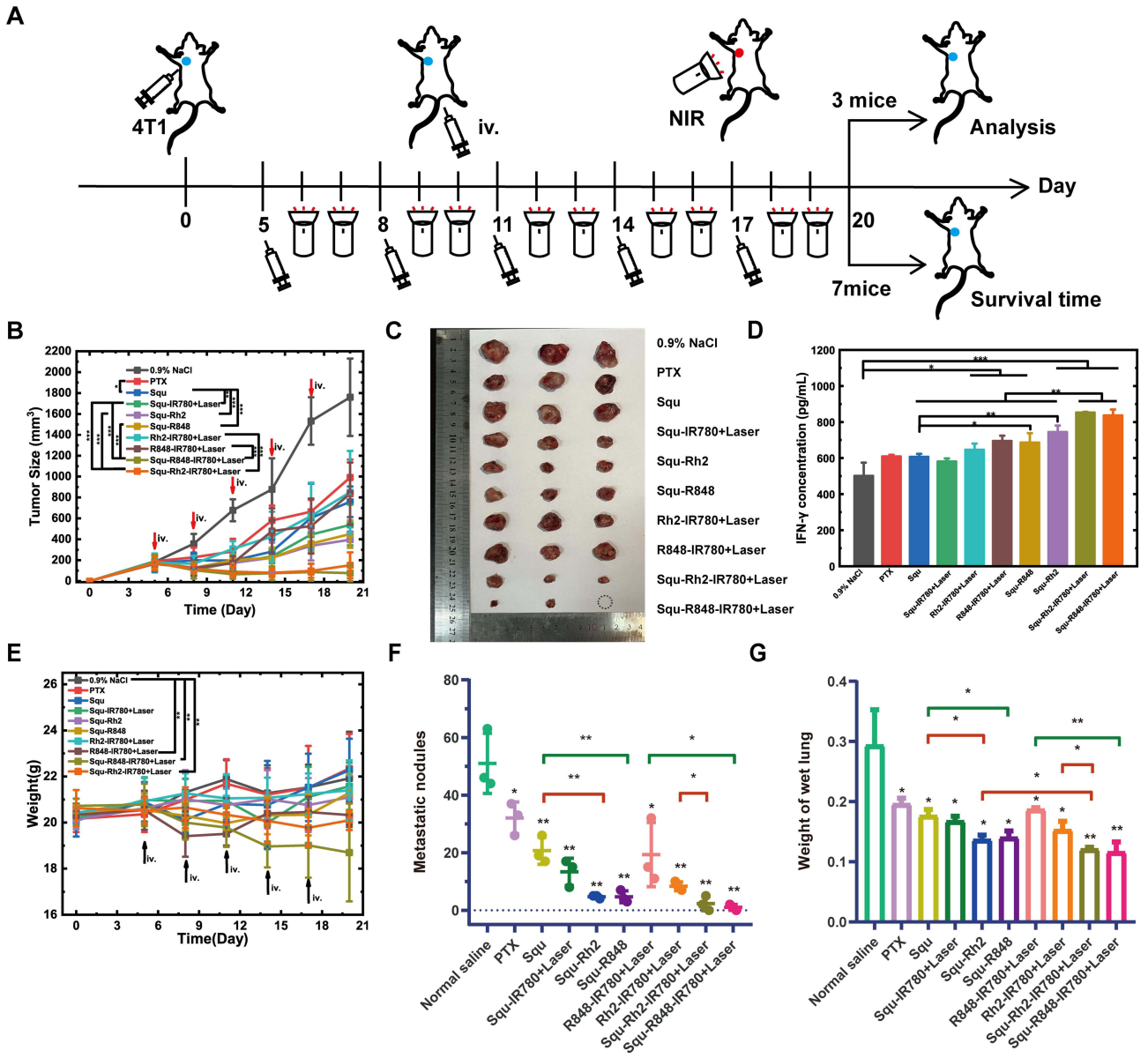

Figure 9 (**A**–**G**) In vivo antitumor therapeutic efficacy investigation. (**A**) Schematic illustration of the dosing regimen of mice. (**B**) Mean tumor volume change in 4T1 tumor-bearing mice during treatment (within 20 days) (n=10). (**C**) Photograph of dissected tumors for each group (n=3). (**D**) The serum IFN-γ concentration for each group (n=3). (**E**) Weight change of 4T1 tumor-bearing mice during treatment (within 20 days) (n=10). (**F**) Number of lung metastatic nodules in each treatment group and (**G**) wet weight of lung tissue in each group (n=3). Data are expressed as the means ± SDs and were tested by *t*-test, **p*<0.05, ***p*<0.01, **p*<0.001.

extensive activation of innate immune cells and regulates immune suppression.[46,47] It activates DCs through a TLR7/8 MyD88-dependent signaling pathway, polarizes TAMs from the M2 phenotype to the M1 phenotype, and induces the secretion of proinflammatory cytokines and chemokines.[48,49]

Figure 9E showed the body weight changes of mice in all of the tested groups within 20 days. The Squ-R848-IR780 NPs group displayed significant body weight loss, followed by the Squ-Rh2-IR780 NPs group and R848-IR780 NPs group, but all of the mice in these groups gradually regained their body weight after drug withdrawal. The abnormally low liver index and spleen index of the three mice sacrificed in the Squ-Rh2-IR780 NPs group and R848-IR780 NPs group were also near the normal level (approximately 5% for the liver index and approximately 4% for the spleen index) when the remnant mice were examined after death in the subsequent observation (Table S7). The subsequent recovery of the decreased spleen index in other groups was also observed. This phenomenon indicated that the side effects of these NPs may be reversible.

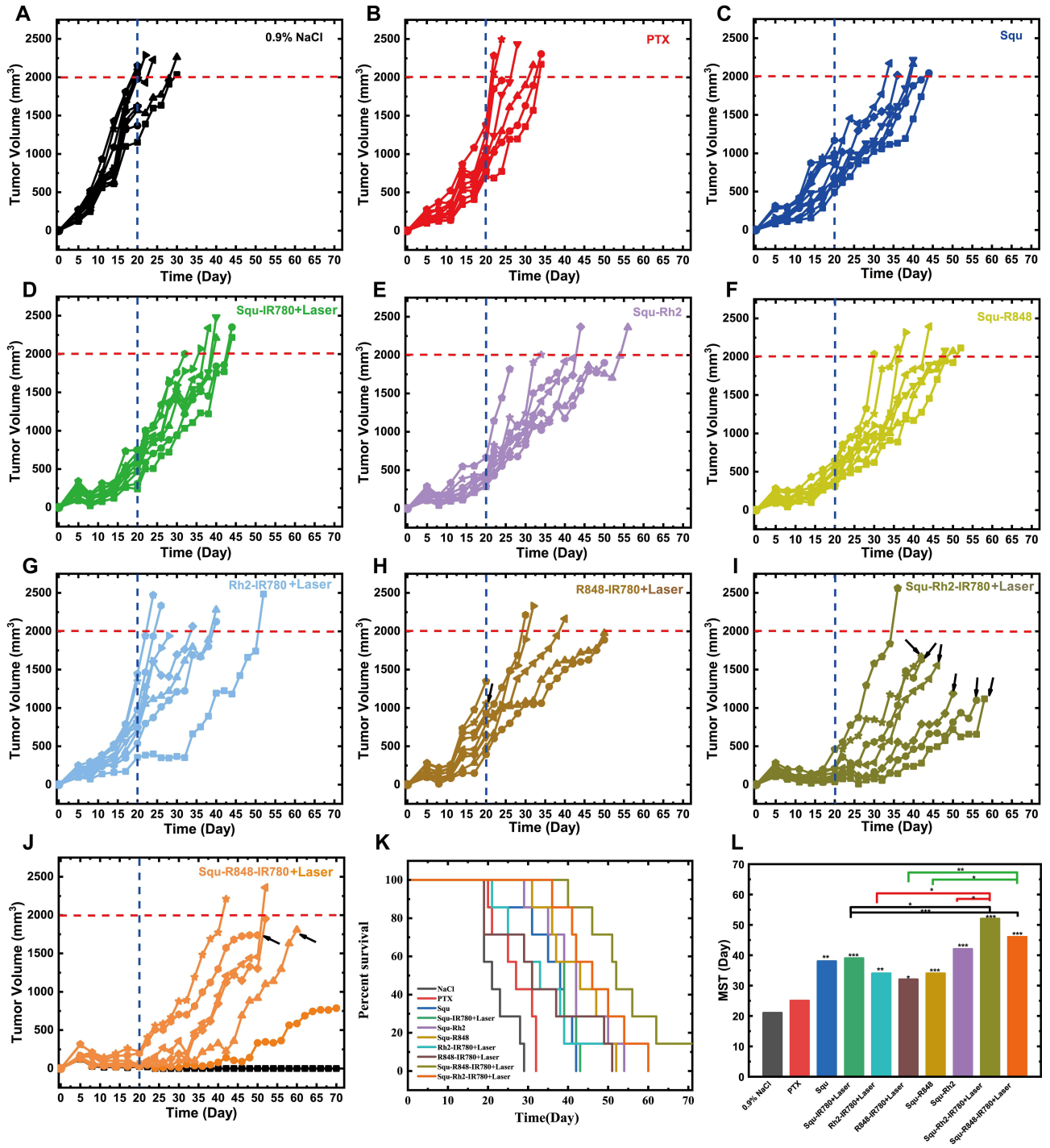

Figure 10 (**A**–**L**) Tumor volume versus time curve. A for 0.9% NaCl group, B for PTX injections group, C for Squ NPs group, D for Squ-IR780 NPs + Laser group, E for Squ-Rh2 NPs group, F for Squ-R848 NPs group, G for Rh2-IR780 NPs + Laser group, H for R848-IR780 NPs + Laser group, I for Squ-Rh2-IR780 NPs + Laser group, J for Squ-R848-IR780 NPs + Laser group. The horizontal red dotted line represents the tumor volume reaching 2000 mm^3, and the upright blue dotted line represents the end of the treatment. The black line represents the disappearance of the tumor. The black arrows mean the mice natural mortality. (**K**) Percent survival rate and (**L**) the median survival time of mice in each group (n=7). *p<0.05, **p<0.01, *p<0.001.

4T1 is a highly metastatic tumor cell line and is widely used for lung metastasis of breast cancer and related anti-metastasis investigations. In this study, the lung metastasis of the different groups was also examined. An average of 51 lung metastasis nodules were observed in the normal saline group (Figure 9F), which also showed the highest wet lung weight among all of the groups (Figure 9G). Administration of PTX injections displayed a low pulmonary metastasis

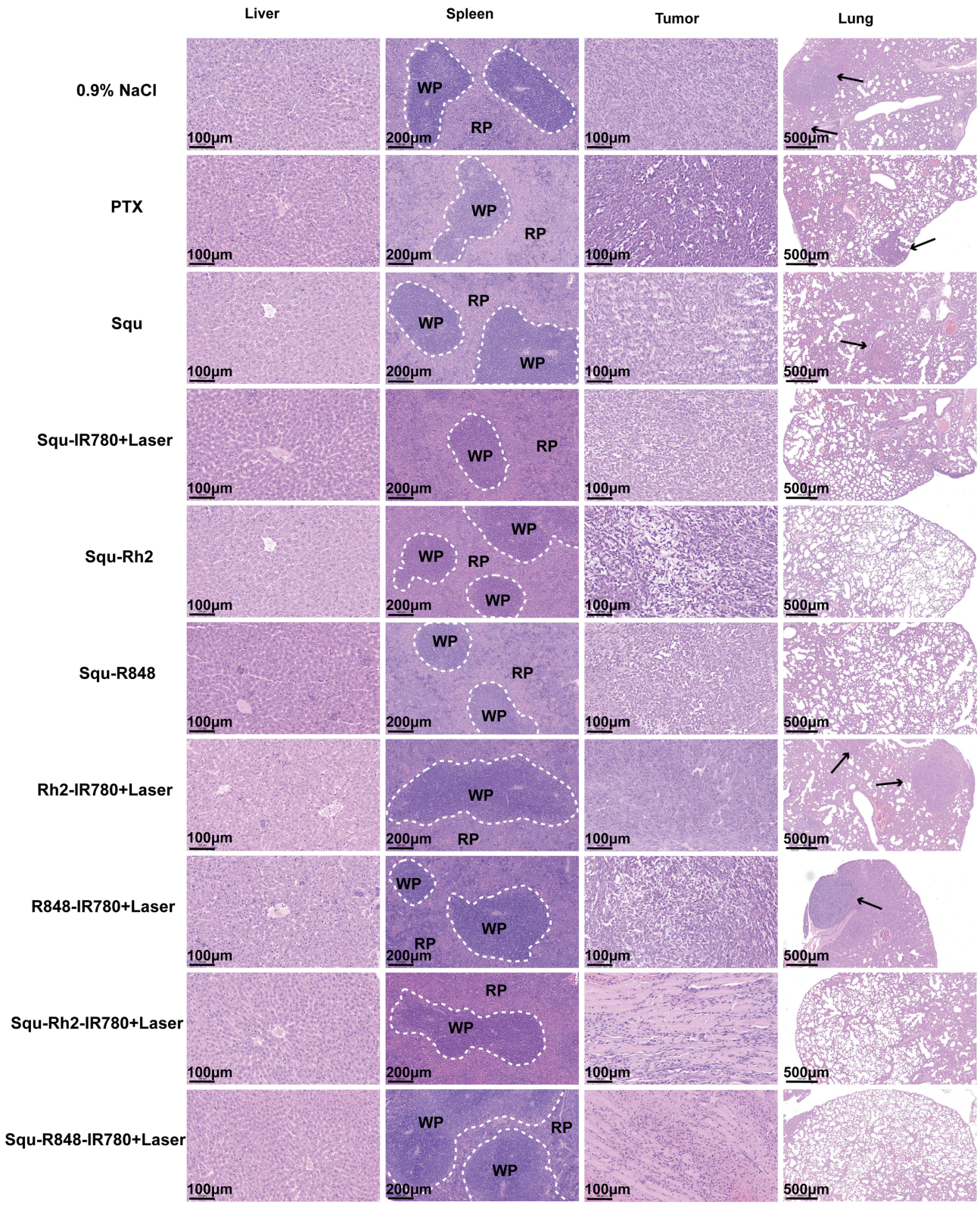

Figure 11 H&E staining of the tumor, lung, liver and spleen of 4T1-bearing mice with subcutaneous tumors after treatment. (liver =100 μm, spleen =200 μm, tumor =100 μm, lung=500 μm). WP represents white pulp, RP represents red pulp, and the black arrow represents the metastatic lesion under the microscope.

inhibition rate (PMIR) of 37.25%. Squ NP treatment reached a PMIR of 59.47%, and further combined use with IR780 led to a PMIP of 73.86%. Administration of Squ-Rh2 NPs or Squ-R848 NPs resulted in a higher PMIR of nearly 90% (Table S5). The highest PMIP was achieved by treatment with Squ-Rh2-IR780 NPs (95.42%) and Squ-R848-IR780 NPs (98.09%). It seemed that the antimetastatic effect of these NPs was in accordance with their tumor growth inhibitory efficacy. Squ-Rh2-IR780 NPs and Squ-R848-IR780 NPs not only demonstrated extraordinary in vivo antitumor efficacy but also showed super antimetastatic activity and thus were very promising for tumor treatment.

Survival time is another key indicator for antitumor efficacy evaluation. As seen in Table S6 and Figure 10K and L, the mean survival time (MST) was only 21 days for the normal saline group and 25 days for the PTX injection group. The treatment of Squ-containing nanoparticles such as Squ NPs, Squ-IR780 NPs, Squ-Rh2 NPs, Squ-R848 NPs and Squ-Rh2-IR780 NPs reached significantly prolonged MST values of 38 days, 39 days, 42 days, 43 days and 46 days (Table S6), demonstrating that Squ was a promising anti-tumor agent. The longest MST of 52 days, which was 2.08-fold that of PTX injections and 1.37-fold that of Squ NPs, was achieved by treatment with Squ-R848-IR780 NPs. The above results proved that the two multifunctional NPs had excellent therapeutic efficacy against breast cancer.

H&E staining of tumors, livers, lungs and spleens of dissected mice showed that the livers of all groups showed a normal hepatic lobular structure (Figure 11). The central vein was surrounded by hepatocytes, hepatic sinusoids and a normal portal vein. The spleens of mice in the normal saline group as well as the Squ group and Squ-IR780 group showed normal morphology, such as a clear junction between the red pulp (RP) and the white pulp (WP), with the red color of the RP being more conspicuous and the blue color of the WP being more prominent. In contrast to the other groups containing immunoadjuvant, which showed blurring of the boundaries between the WP and the RP with sparse arrangement and WP hyperplasia, displaying a certain degree of pathology, which was in line with the liver, spleen and thymus indices, the results were similar (Table S7). Since the spleen is the largest immune organ of the human body and is responsible for hematopoiesis and the immune response, we suspect that some oxidative damage to the spleen occurs under the action of immune adjuvants,[50,51] which is consistent with the results of the spleen index measured on the 20th day. In the tumor H&E results, in the control group, most of the cells showed a regular spherical morphology, significant anisotropy could be observed in the nuclei, and areas of necrosis were not observed overall, while the rest of the treatment groups showed a certain degree of nuclear consolidation or rupture of the nuclei, and the cells at the tumor site in the Squ-Rh2-IR780 group and the Squ-R848-IR780 group appeared or even showed nucleolysis or disappearance of nuclei, indicating that the most severe cell damage was observed. The above results proved that the two multifunctional NPs had a powerful killing effect on tumor cells. In addition, the lung tissues of the 0.9% NaCl group, PTX injection group, Squ NPs group, Rh2-IR780 NPs group and R848-IR780 NPs group were occupied by tumors, whereas only a very small number of lung nodules were found in the combined treatment group, with clear and intact alveolar structures and the smallest mass of the lungs. It seemed that the antimetastatic effect of these NPs was in accordance with their tumor growth inhibitory efficacy.

Conclusion

We developed two multifunctional Squ-R848-IR780 NPs and Squ-Rh2-IR780 NPs, which combined chemotherapy, photothermal therapy, immunoregulation, in vivo imaging and tumor targetability through coloading squamocin, IR780, R848 or Rh2 into drug carriers composed of OA and PCL_{2000}-$mPEG_{2000}$. Squamocin, a naturally resourced potent anti-tumor agent, demonstrated a synergistic effect with immunoregulators (R848 and Rh2) and IR780. The resultant Squ-R848-IR780 NPs and Squ-Rh2-IR780 NPs achieved extraordinary in vivo therapeutic efficacy (TIR being over 90%, MST being 2-fold more than that of PTX injections) and almost completely inhibited the lung metastasis of breast tumors. Squ-R848-IR780 NPs were slightly more effective than Squ-Rh2-IR780 NPs, but Squ-Rh2-IR780 NPs showed better safety with higher body weight and less abnormal behavior during treatment. Both nanoparticles are worth further investigation, such as formulation optimization or validation in more tumor models, to become effective anti-tumor drugs for practical application in the clinical treatment of tumors.

Abbreviations

Squ, Squamocin; NPs, nanoparticles; TLR, toll-like receptor; R848, resiquimod; EPR, enhancing permeability and retention effect; PPT, photothermal therapy; PDI, polydispersity index; NIR, near infrared; PDT, photodynamic therapy;

TAMs, tumor-associated macrophages; ICD, immunogenic cell death; PTX, paclitaxel; $mPEG_{2k}$-PCL_{2k}, monomethoxyl [poly(ethylene glycol)2000]-b-[poly (ε-caprolactone)2000]; OA, oleic acid; HPLC, high-performance liquid chromatography; TEM, transmission electron microscopy; DLC, drug loading capacity; EE, encapsulation efficiency; PBS, phosphate buffer saline; RTTI, relative tumor targeting index; TIR, tumor inhibition rate; H&E, hematoxylin and eosin; PMIR, pulmonary metastasis inhibition rate; PCE, photothermal conversion efficiency; RP, red pulp; WP, white pulp; APCs, antigen-presenting cells; TAMs, tumor-associated macrophages; DAMPs, damage associated molecular patterns; TME, tumor microenvironment.

Ethics Approval and Informed Consent

All animal experiments are conducted in accordance with the Ethical and Regulatory Guidelines for Animal Experiments formulated by the Chinese Institute for the Development of Medicinal Plants (IMPLAD). IMPLAD's ethics committee gave the study ethical approval.

Author Contributions

All authors made a significant contribution to the work reported, whether that is in the conception, study design, execution, acquisition of data, analysis and interpretation, or in all these areas; took part in drafting, revising or critically reviewing the article; gave final approval of the version to be published; have agreed on the journal to which the article has been submitted; and agree to be accountable for all aspects of the work.

Funding

This research was funded by the CAMS Innovation Fund for Medical Sciences (CIFMS) (No. 2021-I2M-1–071).

Disclosure

The authors have declared no competing interests in this work.

References

1. Chaudhuri A, Kumar DN, Dehari D, et al. Endorsement of TNBC biomarkers in precision therapy by nanotechnology. *Cancers*. 2023;15(9):2661. doi:10.3390/cancers15092661
2. Park JH, Pyun WY, Park HW. Cancer metabolism: phenotype, signaling and therapeutic targets. *Cells*. 2020;9(10):2308. doi:10.3390/cells9102308
3. Kashyap D, Garg VK, Goel N. Intrinsic and extrinsic pathways of apoptosis: role in cancer development and prognosis. *Adv Protein Chem Struct Biol*. 2021;125:73–120.
4. Zhang Y, Zhang Z. The history and advances in cancer immunotherapy: understanding the characteristics of tumor-infiltrating immune cells and their therapeutic implications. *Cell Mol Immunol*. 2020;17(8):807–821. doi:10.1038/s41423-020-0488-6
5. Loibl S, Poortmans P, Morrow M, Denkert C, Curigliano G. Breast cancer. *Lancet*. 2021;397(10286):1750–1769. doi:10.1016/S0140-6736(20)32381-3
6. Zannetti A. Breast cancer: from pathophysiology to novel therapeutic approaches 2.0. *Int J Mol Sci*. 2023;24(3):2542. doi:10.3390/ijms24032542
7. Gajewski TF, Schreiber H, Fu YX. Innate and adaptive immune cells in the tumor microenvironment. *Nat Immunol*. 2013;14(10):1014–1022. doi:10.1038/ni.2703
8. Shao K, Singha S, Clemente-Casares X, Tsai S, Yang Y, Santamaria P. Nanoparticle-based immunotherapy for cancer. *ACS Nano*. 2015;9(1):16–30. doi:10.1021/nn5062029
9. Shi Y, van der Meel R, Chen X, Lammers T. The EPR effect and beyond: strategies to improve tumor targeting and cancer nanomedicine treatment efficacy. *Theranostics*. 2020;10(17):7921–7924. doi:10.7150/thno.49577
10. Mitchell MJ, Billingsley MM, Haley RM, Wechsler ME, Peppas NA, Langer R. Engineering precision nanoparticles for drug delivery. *Nat Rev Drug Discov*. 2021;20(2):101–124. doi:10.1038/s41573-020-0090-8
11. Gao Y, Wang K, Zhang J, Duan X, Sun Q, Men K. Multifunctional nanoparticle for cancer therapy. *Med Comm*. 2023;4(1):e187.
12. Gupta J, Safdari HA, Hoque M. Nanoparticle mediated cancer immunotherapy. *Semin Cancer Biol*. 2021;69:307–324. doi:10.1016/j.semcancer.2020.03.015
13. Hanley TM, Vankayala R, Mac JT, Lo DD, Anvari B. Acute immune response of micro- and nanosized erythrocyte-derived optical particles in healthy mice. *Mol Pharm*. 2020;17(10):3900–3914. doi:10.1021/acs.molpharmaceut.0c00641
14. Chen Q, Hu Q, Dukhovlinova E, et al. Photothermal therapy promotes tumor infiltration and antitumor activity of CAR T cells. *Adv Mater*. 2019;31(23):e1900192.
15. Salomão EA, Nascimento VAD, de Oliveira CFR, Silva IS, Guimarães RCA, Bogo D. Investigating effects of IR-780 in animal models of B16-F10 melanoma: new approach in lung metastasis. *Molecules*. 2023;28(19):6942. doi:10.3390/molecules28196942
16. Zheng J, Sun Y, Long T, et al. Sonosensitizer nanoplatform-mediated sonodynamic therapy induced immunogenic cell death and tumor immune microenvironment variation. *Drug Delivery*. 2022;29(1):1164–1175. doi:10.1080/10717544.2022.2058653

17. Huang PY, Zhu YY, Zhong H, et al. Autophagy-inhibiting biomimetic nanodrugs enhance photothermal therapy and boost antitumor immunity. *Biomater Sci*. 2022;10(5):1267–1280. doi:10.1039/D1BM01888D
18. Hou X, Tao Y, Pang Y, Li X, Jiang G, Liu Y. Nanoparticle-based photothermal and photodynamic immunotherapy for tumor treatment. *Int J Cancer*. 2018;143(12):3050–3060. doi:10.1002/ijc.31717
19. Ye J, Mills BN, Qin SS, et al. Toll-like receptor 7/8 agonist R848 alters the immune tumor microenvironment and enhances SBRT-induced antitumor efficacy in murine models of pancreatic cancer. *J Immunother Cancer*. 2022;10(7):e004784. doi:10.1136/jitc-2022-004784
20. Li X, Chu S, Lin M, et al. Anticancer property of ginsenoside Rh2 from ginseng. *Eur J Med Chem*. 2020;203:112627. doi:10.1016/j.ejmech.2020.112627
21. Xiaodan S, Ying C. Role of ginsenoside Rh2 in tumor therapy and tumor microenvironment immunomodulation. *Biomed Pharmacother*. 2022;156:113912. doi:10.1016/j.biopha.2022.113912
22. Chen Q, Zhang L, Li L, et al. Cancer cell membrane-coated nanoparticles for bimodal imaging-guided photothermal therapy and docetaxel-enhanced immunotherapy against cancer. *J Nanobiotechnol*. 2021;19(1):449. doi:10.1186/s12951-021-01202-x
23. Jiang M, Zeng J, Zhao L, et al. Chemotherapeutic drug-induced immunogenic cell death for nanomedicine-based cancer chemo-immunotherapy. *Nanoscale*. 2021;13(41):17218–17235. doi:10.1039/D1NR05512G
24. Duval RA, Lewin G, Peris E, et al. Heterocyclic analogues of squamocin as inhibitors of mitochondrial complex I. On the role of the terminal lactone of annonaceous acetogenins. *Biochemistry*. 2006;45(8):2721–2728. doi:10.1021/bi051261u
25. Lee CC, Lin YH, Chang WH, Lin PC, Wu YC, Chang JG. Squamocin modulates histone H3 phosphorylation levels and induces G1 phase arrest and apoptosis in cancer cells. *BMC Cancer*. 2011;11(1):58. doi:10.1186/1471-2407-11-58
26. Raynaud S, Némati F, Miccoli L, et al. Antitumoral effects of squamocin on parental and multidrug resistant MCF7 (human breast adenocarcinoma) cell lines. *Life Sci*. 1999;65(5):525–533. doi:10.1016/S0024-3205(99)00273-8
27. Chen Y, Chen JW, Wang Y, Xu SS, Li X. Six cytotoxic annonaceous acetogenins from Annona squamosa seeds. *Food Chem*. 2012;135(3):960–966. doi:10.1016/j.foodchem.2012.05.041
28. Kim EJ, Suh KM, Kim DH, et al. Asimitrin and 4-hydroxytrilobin, new bioactive annonaceous acetogenins from the seeds of Asimina triloba possessing a bis-tetrahydrofuran ring. *J Nat Prod*. 2005;68(2):194–197. doi:10.1021/np040184l
29. Gonçalves ASC, Rodrigues CF, Fernandes N, et al. IR780 loaded gelatin-PEG coated gold core silica shell nanorods for cancer-targeted photothermal/photodynamic therapy. *Biotechnol Bioeng*. 2022;119(2):644–656. doi:10.1002/bit.27996
30. Fu J, Wang Y, Li H, et al. A simple but efficient tumor-targeted nanoparticle delivery system constructed by oleic acid. *Drug Delivery*. 2022;29(1):2539–2548. doi:10.1080/10717544.2022.2105447
31. Liu Y, Yang G, Jin S, Xu L, Zhao C-X. Development of High-Drug-Loading Nanoparticles. *Chem Plus Chem*. 2020;85(9):2143–2157. doi:10.1002/cplu.202000496
32. Ren W, Yan Y, Zeng L, et al. A near infrared light triggered hydrogenated black TiO2 for cancer photothermal therapy. *Adv Healthc Mater*. 2015;4(10):1526–1536. doi:10.1002/adhm.201500273
33. Luo S, Wang Y, Shen S, et al. IR780-loaded hyaluronic Acid@Gossypol–Fe(III)–EGCG infinite coordination polymer nanoparticles for highly efficient tumor photothermal/coordinated dual drugs synergistic therapy. *Adv Funct Mater*. 2021;31(24):2100954. doi:10.1002/adfm.202100954
34. Zhao X, Zhao H, Wang S, et al. A tumor-targeting near-infrared heptamethine cyanine photosensitizer with twisted molecular structure for enhanced imaging-guided cancer phototherapy. *J Am Chem Soc*. 2021;143(49):20828–20836. doi:10.1021/jacs.1c09155
35. Yuan Z, He H, Zou J, et al. Polydopamine-coated ferric oxide nanoparticles for R848 delivery for photothermal immunotherapy in breast cancer. *Int J Pharm*. 2023;644:123249. doi:10.1016/j.ijpharm.2023.123249
36. Melancon MP, Elliott AM, Shetty A, Huang Q, Stafford RJ, Li C. Near-infrared light modulated photothermal effect increases vascular perfusion and enhances polymeric drug delivery. *J Control Release*. 2011;156(2):265–272. doi:10.1016/j.jconrel.2011.06.030
37. Hua S, He J, Zhang F, et al. Multistage-responsive clustered nanosystem to improve tumor accumulation and penetration for photothermal/enhanced radiation synergistic therapy. *Biomaterials*. 2021;268:120590. doi:10.1016/j.biomaterials.2020.120590
38. Wang Q, Liang Q, Dou J, et al. Breaking through the basement membrane barrier to improve nanotherapeutic delivery to tumours. *Nat Nanotechnol*. 2023;19(1):95–105.
39. Lv Y, Li F, Wang S, et al. Near-infrared light-triggered platelet arsenal for combined photothermal-immunotherapy against cancer. *Sci Adv*. 2021;7(13). doi:10.1126/sciadv.abd7614
40. Song CW, Park H, Griffin RJ. Improvement of tumor oxygenation by mild hyperthermia. *Radiat Res*. 2001;155(4):515–528. doi:10.1667/0033-7587(2001)155[0515:IOTOBM]2.0.CO;2
41. Tan B, Wu Y, Wu Y, et al. Curcumin-Microsphere/IR820 hybrid bifunctional hydrogels for in situ osteosarcoma chemo-co-thermal therapy and bone reconstruction. *ACS Appl Mater Interfaces*. 2021;13(27):31542–31553. doi:10.1021/acsami.1c08775
42. Ojha T, Pathak V, Shi Y, et al. Pharmacological and physical vessel modulation strategies to improve EPR-mediated drug targeting to tumors. *Adv Drug Deliv Rev*. 2017;119:44–60. doi:10.1016/j.addr.2017.07.007
43. Li X, Lovell JF, Yoon J, Chen X. Clinical development and potential of photothermal and photodynamic therapies for cancer. *Nat Rev Clin Oncol*. 2020;17(11):657–674. doi:10.1038/s41571-020-0410-2
44. Dewey WC, Thrall DE, Gillette EL. Hyperthermia and radiation--a selective thermal effect on chronically hypoxic tumor cells in vivo. *Int J Radiat Oncol Biol Phys*. 1977;2(1–2):99–103. doi:10.1016/0360-3016(77)90013-X
45. Westermann AM, Jones EL, Schem BC, et al. First results of triple-modality treatment combining radiotherapy, chemotherapy, and hyperthermia for the treatment of patients with stage IIB, III, and IVA cervical carcinoma. *Cancer*. 2005;104(4):763–770. doi:10.1002/cncr.21128
46. Wang B, Van Herck S, Chen Y, et al. Potent and prolonged innate immune activation by enzyme-responsive imidazoquinoline TLR7/8 agonist prodrug vesicles. *J Am Chem Soc*. 2020;142(28):12133–12139. doi:10.1021/jacs.0c01928
47. Michaelis KA, Norgard MA, Zhu X, et al. The TLR7/8 agonist R848 remodels tumor and host responses to promote survival in pancreatic cancer. *Nat Commun*. 2019;10(1):4682. doi:10.1038/s41467-019-12657-w
48. Rodell CB, Arlauckas SP, Cuccarese MF, et al. TLR7/8-agonist-loaded nanoparticles promote the polarization of tumour-associated macrophages to enhance cancer immunotherapy. *Nat Biomed Eng*. 2018;2(8):578–588. doi:10.1038/s41551-018-0236-8
49. Hemmi H, Kaisho T, Takeuchi O, et al. Small anti-viral compounds activate immune cells via the TLR7 MyD88-dependent signaling pathway. *Nat Immunol*. 2002;3(2):196–200. doi:10.1038/ni758

50. Barzilai A, Yamamoto K. DNA damage responses to oxidative stress. *DNA Repair*. 2004;3(8–9):1109–1115. doi:10.1016/j.dnarep.2004.03.002
51. Miyata T, Takamura H, Kin R, et al. Spleen volume as a predictive biomarker for thrombocytopenia and liver dysfunction after oxaliplatin-based chemotherapy. *Anticancer Res*. 2020;40(6):3361–3370. doi:10.21873/anticanres.14319